coatings

MDPI

Article

# Effect of Initial Surface Roughness on Cavitation Erosion Resistance of Arc-Sprayed Fe-Based Amorphous/Nanocrystalline Coatings

**Jinran Lin [1,2,3,*], Zehua Wang [2], Jiangbo Cheng [2], Min Kang [1], Xiuqing Fu [1] and Sheng Hong [2,4]**

1 College of Engineering, Nanjing Agricultural University, Nanjing 210031, China; kangmin@njau.edu.cn (M.K.); fuxiuqing@njau.edu.cn (X.F.)
2 College of Mechanics and Materials, Hohai University, Nanjing 211100, China; zhwang@hhu.edu.cn (Z.W.); jiangbochenghhu@hotmail.com (J.C.); hongsheng1988@126.com (S.H.)
3 Jiangsu Jinxiang Transmission Equipment Co., Ltd., Huaian 223001, China
4 Material Corrosion and Protection Key Laboratory of Sichuan Province, Zigong 643000, China
* Correspondence: ljr-8@163.com; Tel.: +86-25-5860-6580

Academic Editor: Shiladitya Paul
Received: 23 September 2017; Accepted: 1 November 2017; Published: 14 November 2017

**Abstract:** The arc spraying process was used to prepare Fe-based amorphous/nanocrystalline coating. The cavitation erosion behaviors of FeNiCrBSiNbW coatings with different surface roughness levels were investigated in distilled water. The results showed that FeNiCrBSiNbW coating adhered well to the substrate, and was compact with porosity of less than 2%. With increasing initial surface roughness, the coatings showed an increase in mass loss of cavitation erosion damage. The amount of pre-existing defects on the initial surface of the coatings was found to be a significant factor for the difference in the cavitation erosion behavior. The cavitation erosion damage for the coatings was a brittle erosion mode. The evolution of the cavitation erosion mechanism of the coatings with the increase of the initial surface roughness was micro-cracks, pits, detachment of fragments, craters, cracks, pullout of the un-melted particle, and massive exfoliations.

**Keywords:** cavitation; roughness; coatings; amorphous/nanocrystalline; Fe-based

## 1. Introduction

Cavitation erosion, often reported as a common phenomenon in the overflowing components of hydraulic machinery, is related to two main aspects of hydrodynamic and material [1,2]. On the one hand, hydrodynamic cavitation takes place when vapor bubbles in a liquid are exposed to a sudden fluctuation of localized pressure, which can cause repeated nucleation, growth, violent collapse of bubbles, and send micro-jet or shock wave through the liquid to the solid surfaces [3]. Thus, surface roughness is capable of controlling cavitation erosion by affecting nuclei concentration, turbulence level and surface pressure distribution [4,5]. On the other hand, it is important to prepare a high performance coating to reduce or avoid cavitation erosion damage by selecting a suitable surface treatment technique, since cavitation erosion usually happens on a material surface of the flow-handling components such as hydraulic turbines, offshore/mining machineries, valves, and ship propellers [6–8].

Fe-based amorphous/nanocrystalline coatings prepared by thermal spraying have been widely adopted by hydraulic machinery, power plants and coastal installations because of their desirable combination of relatively low material cost, high hardness and toughness, and outstanding corrosion and wear resistance [9–12]. In recent years, considerable efforts have

been devoted to investigate the cavitation erosion behavior of Fe-based amorphous/nanocrystalline coatings [13–21]. According to [13,18], the high-velocity oxygen-fuel (HVOF) sprayed Fe-based amorphous/nanocrystalline coatings with dense structure and high microhardness were preferable to improve the resistance of cavitation erosion in deionized water. In addition, both porosity and microhardness affected the cavitation erosion resistance of HVOF sprayed coatings [18–20]. The influence of the HVOF spray parameters has also been investigated in relation to the microstructure and hardness of the coatings and, in turn, the cavitation erosion resistance [21]. Compared with HVOF spraying, arc spraying has the potential to develop high quality Fe-based amorphous/nanocrystalline coatings with lower costs because of its advantages of simple device, flexible operation and high efficiency [22]. In our earlier studies, FeCrBSiNb(Ni/W) amorphous/nanocrystalline coatings were synthesized successfully using the arc spraying process and their cavitation erosion behavior was reported [16,17]. We demonstrated that the cavitation erosion resistance of arc-sprayed Fe-based amorphous/nanocrystalline coating deteriorated with increasing annealing temperature [11]. Previous investigations mainly described in detail the relationship among microstructure, mechanical properties and cavitation erosion resistance of the Fe-based amorphous/nanocrystalline coatings. However, the role that initial surface roughness plays in cavitation erosion process of arc-sprayed Fe-based amorphous/nanocrystalline coatings is still not clear. In particular, thermal sprayed coating possessed of non-uniform microstructure and its top layers close to surface showed higher porosity than the underneath layers, which was different from bulk metal.

The aim of this study was to discover the effect of initial surface roughness on cavitation erosion behavior of FeNiCrBSiNbW amorphous/nanocrystalline coating prepared by arc spraying process. Moreover, the mechanisms controlling cavitation erosion of the coatings with different initial surface roughness were discussed.

## 2. Experimental Procedure

A self-designed Fe-based cored wire (Fe-Ni-Cr-B-Si-Nb-W) with a diameter of 2 mm was used as the feedstock. The chemical composition of the cored wire was the same in Ref [17]. Stainless steel 1Cr18Ni9Ti was selected as the substrate. Prior to coating, the substrate samples were pre-cleaned in acetone, dried in hot air, and then grit blasted with 16 mesh alumina to provide a fresh and rough surface for better adhesion by removing all rust and oxide skin. The substrate samples were cooled with compressed air jets during and after spraying. The arc spraying of the cored wire was carried out at a spraying voltage of 36 V, a spraying current of 120 A, a wire feed rate of 2.7 $m \cdot min^{-1}$, a compressed air pressure of 700 kPa, a stand-off distance of 200 mm, and a gun traverse speed of 100 $mm \cdot s^{-1}$. The thickness of tested coating was about 230 μm. Then, the coating samples were wire cut for microstructural characterization and cavitation erosion testing.

The microstructures of the coating were observed using a scanning electron microscope (SEM, Hitachi S-3400 N, Tokyo, Japan) equipped with an energy dispersive spectroscopy (EDS, EX250). Selected area electron diffraction (SAED) pattern and finer-scale microstructural characterization of the coating were performed using a transmission electron microscope (TEM, JEOL JEM-2010, Tokyo, Japan). Porosity was measured on SEM images with the help of image analysis. An average value was taken from 20 view-fields from different locations on polished cross section of the coating at a magnification of 500.

The cavitation erosion experiments of the coatings were carried out using a vibratory cavitation apparatus according to the ASTM G32-10 standard [23]. The operating parameters of the cavitation test were as follows: Frequency of vibration 19 ± 1 kHz, peak-to-peak amplitude 60 ± 5 μm, power of ultrasonic generator 250 W. The details of the cavitation erosion test apparatus and its specimen's dimension have been reported in Ref. [16]. In this work, three surface roughness levels of the coating samples were prepared by manual grinding using 80, 600 and 1000 grit silicon carbide papers, which cause a large difference in the initial surface roughness and magnify its effect on the cavitation erosion behavior. Moreover, the initial surface roughness values of the coating samples ground using 600 and 1000 grit silicon carbide papers were close to the surface roughness of steam turbine blades after

surface finish [24]. Prior to the test, the coating samples with an average initial surface roughness values ($R_a$) of 0.89, 0.32 and 0.2 μm were cleaned with acetone in an ultrasonic bath, dried in hot air, and weighed by an analytical balance with an accuracy of 0.1 mg. Then, the screw specimen with the Fe-based amorphous/nanocrystalline coating on it was attached to the free end of the horn and immersed about 3 mm in distilled water. The beaker was surrounded by flowing cool water to keep the distilled water inside it at 25 ± 5 °C. After each test period, the specimen was removed from the tip, cleaned with acetone, dried in hot air and weighted. The eroded surface morphologies of the coatings were characterized by SEM. Each test was repeated thrice to ensure the reproducibility and validity of the experiment results.

## 3. Results and Discussion

### *3.1. Characterization of the Coating*

Figure 1 shows the cross-sectional microstructure of the FeNiCrBSiNbW amorphous/nanocrystalline coating deposited by arc spraying. From the overall view of the coating in Figure 1a, it can be seen that the coating has a dense and typical lamellar structure with an average thickness of 230 μm. The whole coating exhibits an apparent good adherence to the substrate with presence of a uniform and compact interface located between the substrate and the coating. It is notable in Figure 1b that some pores, un-melted particles and microcracks are observed in the coating. The average porosity value of the coating is less than 2% by using image analysis. Besides the pores, appearing as black regions, the coating consists of bright white region, grey region and dark grey region. The grey region is primarily coating alloy with the chemical composition of $Fe_{71}Ni_5Cr_{15}B_3Si_3Nb_2W_1$ (at.%). The bright white region and the dark grey region are W-rich phase and iron oxide phase respectively, which is in accordance with the results observed in previous work [25].

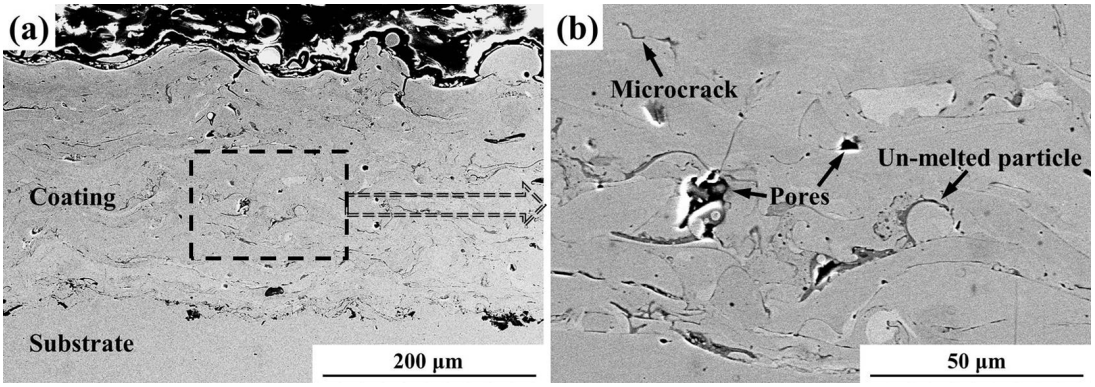


**Figure 1.** Scanning electron microscope (SEM) images of a transverse section of the as-sprayed coating: (**a**) an overall view morphology, and (**b**) a magnification of the rectangular frame in Figure 1a.

To get insight into the detailed microstructural information of the FeNiCrBSiNbW amorphous/nanocrystalline coating, TEM was utilized. Figure 2 shows a typical bright field TEM image of the coating, indicating the coexistence of amorphous phase and nanocrystalline grains. The nanocrystalline grains with dimensions ranging from 70 nm to 130 nm are uniformly distributed in amorphous matrix. This is confirmed by the diffraction spots, and the diffused halo rings in the selected area electron diffraction (SAED) pattern, as shown in the inset of Figure 2. The presence of amorphous phase is due to both the multicomponent alloy system with large glass formation ability and the high cooling rates of the in-flight particles. The formation of nanocrystalline grains is attributed to crystallization of the original amorphous region due to the preferred oxidation on the in-flight particles surface and the thermal fluctuation leading to localized heating during successive spraying [26,27].

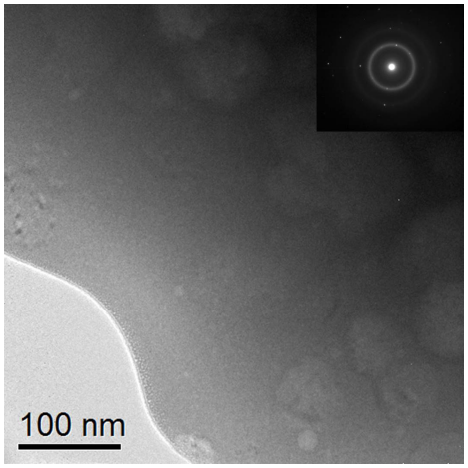


**Figure 2.** Transmission electron microscope (TEM) images of typical microstructure of the as-sprayed coating: Coexistence of amorphous phase and nanocrystalline grains.

### *3.2. Cavitation Erosion Behavior of the Coatings*

Figure 3 shows the relationship between cumulative mass loss and cavitation erosion time for the FeNiCrBSiNbW amorphous/nanocrystalline coatings with three surface roughness levels. The results show that there is a considerable difference in mass loss rate of the as-sprayed coatings under three different surface conditions (i.e., 80, 600, and 1000 grit grinding), although the mass losses of all three coating specimens increase with increasing the test time. The incubation period is not observed for all three coating specimens, which reflects that the surface conditions in this study put the coatings one step ahead into the cavitation erosion damage process. The coating after 80 grit grinding exhibits the greater mass loss (21.8 mg) while the coating after 1000 grit grinding has the lower mass loss (10.3 mg) after 120 min test. In addition, the mass loss data of the coating after 600 grit grinding are very close to that of the coating after 1000 grit grinding during the first 30 min, but gradually higher than those of the coating after 1000 grit grinding when the test time exceeds 30 min. This may be because that a higher surface roughness level is helpful to increase the density of bubble nucleation near the surface of the coating specimen [28,29], which causes more impacts of the collapsing bubble on the surface and then much more mass loss of the coating.

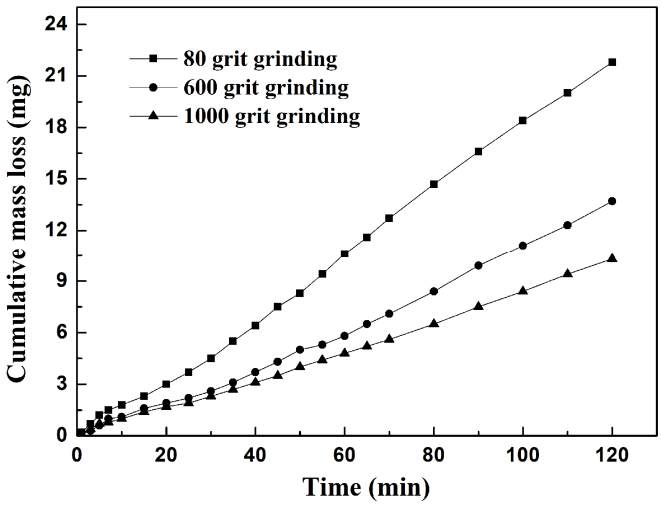


**Figure 3.** The relationship between cumulative mass loss and cavitation erosion time for the as-sprayed coatings with three surface roughness levels.

Figure 4 shows the initial surface morphological features of the FeNiCrBSiNbW amorphous/nanocrystalline coatings under three different surface conditions before the cavitation erosion test. As shown in Figure 4a, many scratches, pits and asperities are observed on the surface of the coating after 80 grit grinding. In Figure 4b, it can be noticed that the surface of the coating after 600 grit grinding is relatively smooth with some small scratches and a small number of irregular pits. The surface of the coating after 1000 grit grinding (Figure 4c) contains tiny scratches and limited pits compared to Figure 4a,b. This is consistent with the surface roughness result, where the Ra of the coating after 1000 grit grinding (0.2 μm) is about 22.9% and 62.5% that of the coatings after 80 grit grinding (0.89 μm) and 600 grit grinding (0.32 μm), respectively. Pre-existing irregular defects such as scratches, pits and asperities those resulted from surface preparation could act as raisers for stresses induced due to the direct impact and the lateral outflow of the micro-jets during successive cavitation process [30], which may suggest that the initial surface roughness plays a great role on the cavitation erosion damage of the coatings. This is verified by the SEM images of eroded surfaces as shown in Figure 5. Other than the initial surface roughness of the coating, the microstructure and phase composition were also important characteristics in determining the cavitation erosion resistance of the coatings. According to our previous study [11], the formation of oxides on the coating surface and between intersplats and the reduction of amorphous phase content would contribute to the decrease of the cavitation erosion resistance. The negative effect of the coating porosity on the cavitation erosion resistance has been indicated by other researchers [13,31].

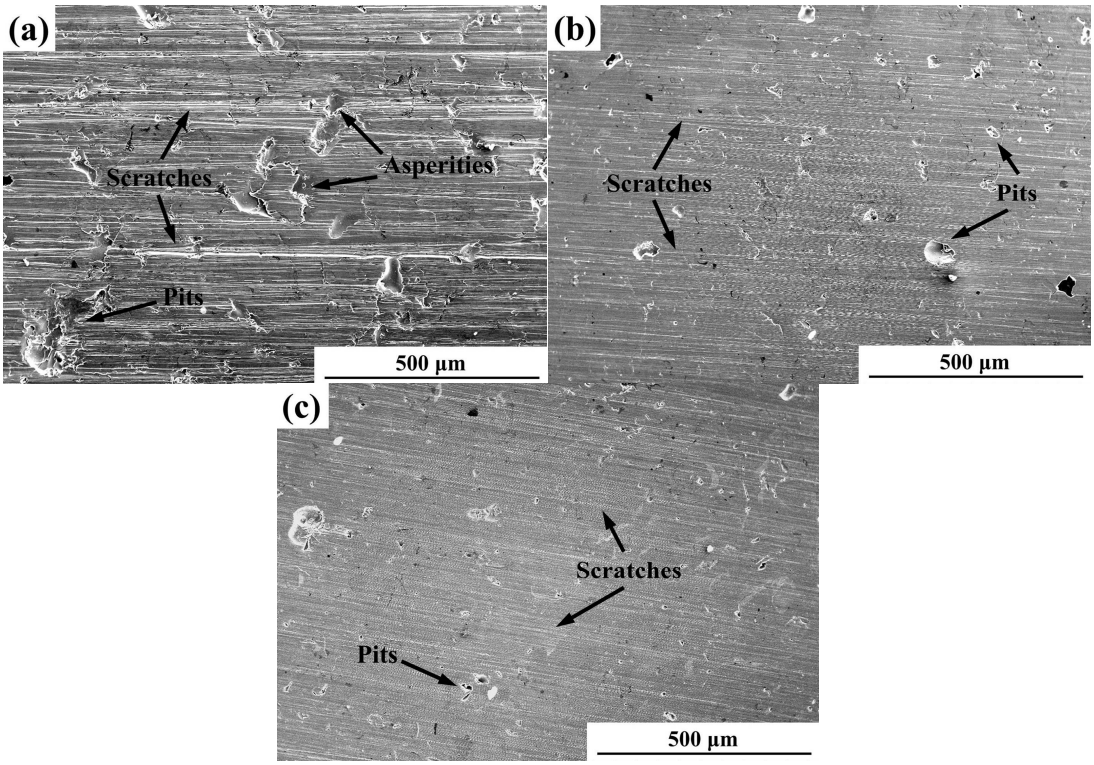


**Figure 4.** SEM images of the surface morphology of as-sprayed coatings under three surface conditions before the cavitation erosion test: (**a**) 80 grit grinding; (**b**) 600 grit grinding; and (**c**) 1000 grit grinding.

Figure 5 shows typical morphological features from the eroded surfaces of the FeNiCrBSiNbW amorphous/nanocrystalline coatings under three different surface conditions after cavitation erosion for 120 min in distilled water. As shown in Figure 5a, the surface of the coating after 80 grit grinding is roughened with a 0.5 mm crater in the center and numerous massive exfoliations of material in a widespread dispersion on the eroded surface, which give contribution to the overall higher mass loss

of the coating. This may be associated with the combination of the initial pits that connected by cracks. Besides, a few initial scratches due to grinding are also observed on the eroded surface. Figure 5b shows a magnified micrograph of the crater with diameter of about 0.5 mm in Figure 5a, where pullout of the un-melted particle, cracks between intersplats, and cleavage fracture with river pattern are detected. These results reveal that the cavitation erosion damage for the coating is a brittle erosion mode. In Figure 5c, it can be noticed that the eroded surface of the coating after 600 grit grinding is relatively smooth with some initial scratches due to grinding. The crater is much shallower compared to Figure 5a, although the area of the crater is relatively larger. Further observation shows that micro-cracks between intersplat and un-melted particle, detachment of fragments, and small amount of pits are recorded on the eroded surface, as shown in Figure 5d. This indicates that the ground surface with lower surface roughness level effectively inhibits the propagation of cracks, hinders the pullout of the un-melted particle, and then delays the cavitation erosion progress of the coating. Figure 5e shows that the eroded surface of the coating after 1000 grit grinding is relatively uniform, including large cracks and number of craters with different shapes. There are also some small pits, micro-cracks, cleavage fracture with river pattern, layer detachment, and a large number of initial tiny scratches and pits due to grinding on the eroded surface (Figure 5f), indicating that it needs more time to roughen the surface and create initiate preferential cavitation erosion initiation sites under the present surface condition. The characteristic of layer detachment on the eroded surface of the coating after 1000 grit grinding reveals that the coating was destroyed mainly in the form of delamination, which was proven in our previous study [17]. From the above results, it may suggest that micro-cracks, pits, detachment of fragments, craters, cracks, pullout of the un-melted particle, and massive exfoliations contribute to the evolution of the cavitation erosion mechanism of the FeNiCrBSiNbW amorphous/nanocrystalline coatings with the increase of the initial surface roughness.

It has been proved by experimental results in the present work that cavitation erosion damage of the coatings became more serious as the initial surface roughness increased. However, it could be expected that the effect of initial surface roughness on the cavitation erosion behavior of the coating is not only dependent on the microstructure of material, but also dependent on the response of surface quality to the impact of micro-jets and shock waves. On the one hand, both the direct impact and the lateral outflow of the micro-jets on the coating surface are influenced by the initial surface roughness. In this manner, the surface of the coating after 80 grit grinding contains more pre-existing defects, as shown in Figure 4a, where nucleation, growth and collapsing of bubbles are more likely to occur [32]. In addition, the rougher surface with more pre-existing defects will entrap the lateral outflow of the water impacts and, in turn, the more cavitation erosion damage of the coating. On the other hand, the cavitation erosion process of the coatings with three initial surface roughness levels may be different. If the impact force of micro-jets and shock waves exceeds the yield stress of the coating, the impacts can plastically deform both the surface and the sub-surface and cause the occurrence of cracks originated from pre-existing defects. It is expected that by increasing the initial surface roughness, there should be an increase in the number of pits per unit of time on the surface of the coating during the cavitation erosion process. In the case of the coating after 1000 grit grinding, the limited pits on the surface merge relatively slowly and form an erosion crater. However, a large amount of pits on the surface of the coating after 80 grit grinding tend to spread over the cavitation erosion region and merge rapidly forming number of craters. With the rebound and implosion of subsequent cavitation bubbles, the un-melted particle peels off, leading to the massive exfoliation of material, as can be seen in Figure 5a,b. It is noteworthy that the amount of pre-existing defects on the initial surface of the FeNiCrBSiNbW amorphous/nanocrystalline coatings has a significant effect on their cavitation erosion behavior.

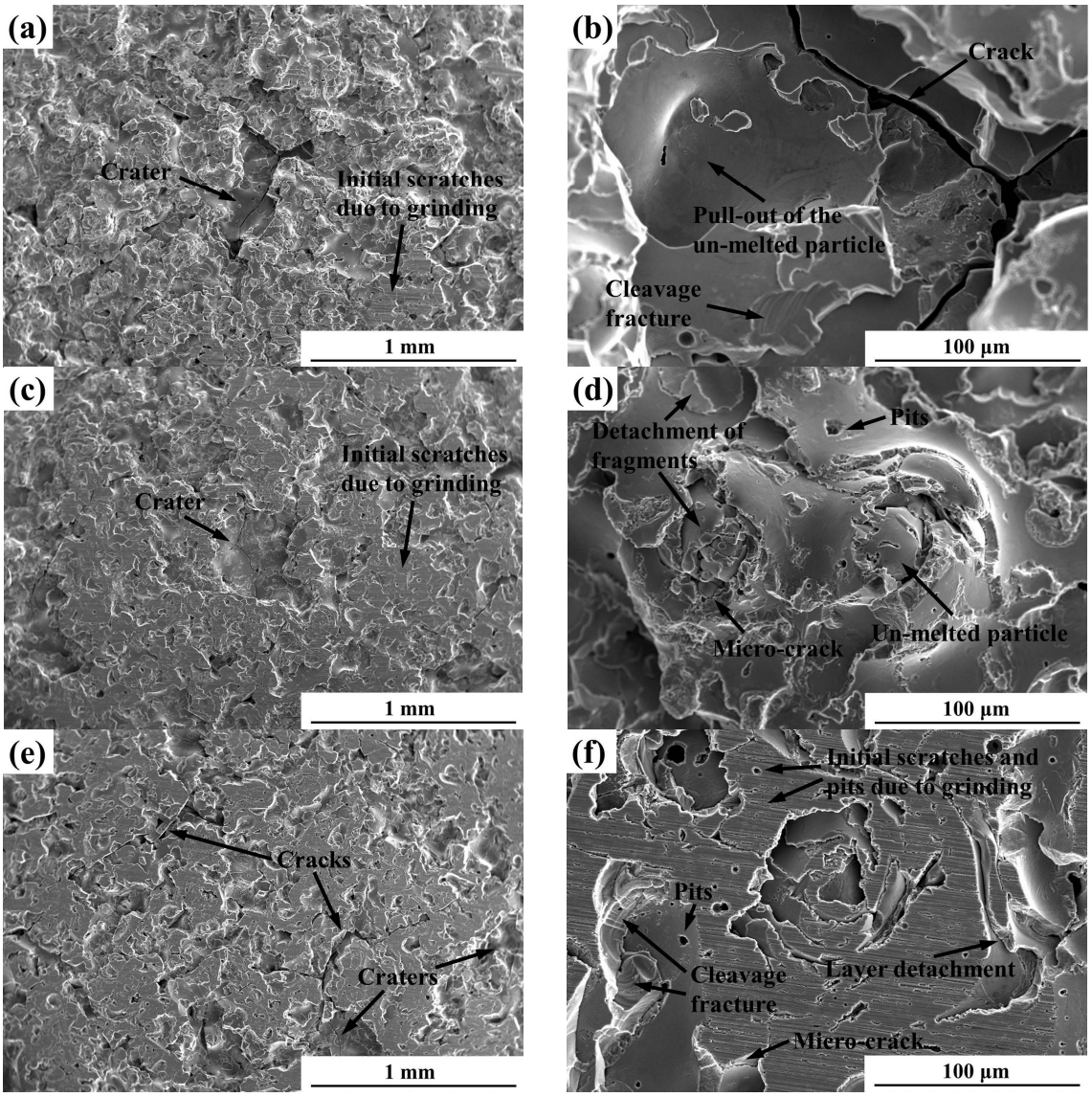


**Figure 5.** SEM images of the surface morphology of as-sprayed coatings under three surface conditions eroded for 120 min: (**a**,**b**) 80 grit grinding; (**c**,**d**) 600 grit grinding; and (**e**,**f**) 1000 grit grinding.

## 4. Conclusions

A FeNiCrBSiNbW coating with amorphous phase and nanocrystalline grains was fabricated using the arc spraying process. The coating had a dense structure with porosity of less than 2% and was adhering well to the substrate. The amount of pre-existing defects on the initial surface of the coatings had a significant effect on the cavitation erosion behavior. With increment of initial surface roughness, the cumulative mass losses of the coatings increased. The coating after 1000 grit grinding exhibited higher cavitation erosion resistance than that of the coating after 80 grit grinding in distilled water. The mechanisms involved in the cavitation erosion process of the coatings with the increase of the initial surface roughness were micro-cracks, pits, detachment of fragments, craters, cracks, pullout of the un-melted particle, and massive exfoliations.

**Acknowledgments:** The research was supported by the Fundamental Research Funds for the Central Universities (Grant Nos. KYZ201660 and RCQD16-04), the China Postdoctoral Science Foundation (Grant No. 2017M621665), the National Natural Science Foundation of China (Grant No. 51609067), the Natural Science Foundation of Jiangsu Province of China (Grant No. BK20150806), and the Opening Project of Material Corrosion and Protection Key Laboratory of Sichuan Province (Grant No. 2016CL08). The authors also gratefully acknowledge the financial support from the Policy-Induced Project of Jiangsu Province for the Industry–University–Research Cooperation (Grant No. BY2015071-02).

**Author Contributions:** Jinran Lin and Zehua Wang conceived and designed the research. Jinran Lin wrote the paper. Jinran Lin and Sheng Hong carried out the experiments. Jiangbo Cheng, Min Kang and Xiuqing Fu entered the discussion.

**Conflicts of Interest:** The authors declare no conflict of interest.

## References

1. Karimi, A.; Martin, J.-L. Cavitation erosion of materials. *Int. Met. Rev.* **1986**, *31*, 1–26. [CrossRef]
2. Wu, C.L.; Zhang, S.; Zhang, C.H.; Zhang, H.; Dong, S.Y. Phase evolution and cavitation erosion-corrosion behavior of FeCoCrAlNiTi$_x$ high entropy alloy coatings on 304 stainless steel by laser surface alloying. *J. Alloys Compd.* **2017**, *698*, 761–770. [CrossRef]
3. Li, D.; Kang, Y.; Wang, X.C.; Ding, X.L.; Fang, Z.L. Effects of nozzle inner surface roughness on the cavitation erosion characteristics of high speed submerged jets. *Exp. Therm. Fluid Sci.* **2016**, *74*, 444–452. [CrossRef]
4. Chiu, K.Y.; Cheng, F.T.; Man, H.C. Evolution of surface roughness of some metallic materials in cavitation erosion. *Ultrasonics* **2005**, *43*, 713–716. [CrossRef] [PubMed]
5. Hutli, E.; Nedeljkovic, M.S.; Bonyar, A.; Radovic, N.A.; Llic, V.; Debeljkovic, A. The ability of using the cavitation phenomenon as a tool to modify the surface characteristics in micro- and in nano-level. *Tribol. Int.* **2016**, *101*, 88–97. [CrossRef]
6. Wang, Y.; Stella, J.; Darut, G.; Poirier, T.; Liao, H.L.; Planche, M.P. APS prepared NiCrBSi-YSZ composite coatings for protection against cavitation erosion. *J. Alloys Compd.* **2017**, *699*, 1095–1103. [CrossRef]
7. Woo, Y.B.; Lee, S.J.; Jeong, J.Y.; Kim, S.J. Evaluation on cavitation characteristics of CoNiCrAlY/$ZrO_2$-$Y_2O_3$ coating layer by atmospheric pressure plasma coating process. *Mater. Res. Bull.* **2014**, *58*, 78–82. [CrossRef]
8. Hong, S.; Wu, Y.P.; Zhang, J.F.; Zheng, Y.G.; Zheng, Y.; Lin, J.R. Synergistic effect of ultrasonic cavitation erosion and corrosion of WC-CoCr and FeCrSiBMn coatings prepared by HVOF spraying. *Ultrason. Sonochem.* **2016**, *31*, 563–569. [CrossRef] [PubMed]
9. Cheng, J.B.; Liang, X.B.; Xu, B.S.; Wu, Y.X. Characterization of mechanical properties of FeCrBSiMnNbY metallic glass coatings. *J. Mater. Sci.* **2009**, *44*, 3356–3363. [CrossRef]
10. Wu, Y.P.; Lin, P.H.; Wang, Z.H.; Li, G.Y. Microstructure and microhardness characterization of a Fe-based coating deposited by high-velocity oxy-fuel thermal spraying. *J. Alloys Compd.* **2009**, *481*, 719–724. [CrossRef]
11. Lin, J.R.; Wang, Z.H.; Lin, P.H.; Cheng, J.B.; Zhang, X.; Hong, S. Effects of post annealing on the microstructure, mechanical properties and cavitation erosion behavior of arc-sprayed FeNiCrBSiNbW coatings. *Mater. Des.* **2015**, *65*, 1035–1040. [CrossRef]
12. Wang, Y.; Li, K.Y.; Scenini, F.; Jiao, J.; Qu, S.J.; Luo, Q.; Shen, J. The effect of residual stress on the electrochemical corrosion behavior of Fe-based amorphous coatings in chloride-containing solutions. *Surf. Coat. Technol.* **2016**, *302*, 27–38. [CrossRef]
13. Wu, Y.P.; Lin, P.H.; Chu, C.L.; Wang, Z.H.; Cao, M.; Hu, J.H. Cavitation erosion characteristics of a Fe-Cr-Si-B-Mn coating fabricated by high velocity oxy-fuel (HVOF) thermal spray. *Mater. Lett.* **2007**, *61*, 1867–1872.
14. Hahn, M.; Fischer, A. Characterization of thermally sprayed micro- and nanocrystalline cylinder wall coatings by means of a cavitation test. *Proc. Inst. Mech. Eng. Part J J. Eng. Tribol.* **2009**, *223*, 27–37. [CrossRef]
15. Hahn, M.; Fischer, A. Characterization of thermal spray coatings for cylinder running surfaces of diesel engines. *J. Therm. Spray Technol.* **2010**, *19*, 866–872. [CrossRef]
16. Wang, Z.H.; Zhang, X.; Cheng, J.B.; Lin, J.R.; Zhou, Z.H. Cavitation erosion resistance of Fe-based amorphous/nanocrystal coatings prepared by high-velocity arc spraying. *J. Therm. Spray Technol.* **2014**, *23*, 742–749. [CrossRef]

17. Lin, J.R.; Wang, Z.H.; Lin, P.H.; Cheng, J.B.; Zhang, X.; Hong, S. Microstructure and cavitation erosion behavior of FeNiCrBSiNbW coating prepared by twin wires arc spraying process. *Surf. Coat. Technol.* **2014**, *240*, 432–436. [CrossRef]
18. Hou, G.L.; Zhao, X.Q.; Zhou, H.D.; Lu, J.J.; An, Y.L.; Chen, J.M.; Yang, J. Cavitation erosion of several oxy-fuel sprayed coatings tested in deionized water and artificial seawater. *Wear* **2014**, *311*, 81–92. [CrossRef]
19. Kim, Y.J.; Jang, J.W.; Lee, D.W.; Yi, S. Porosity effects of a Fe-based amorphous/nanocrystals coating prepared by a commercial high velocity oxy-fuel process on cavitation erosion behaviors. *Met. Mater. Int.* **2015**, *21*, 673–677. [CrossRef]
20. Zheng, Z.B.; Zheng, Y.G.; Sun, W.H.; Wang, J.Q. Effect of heat treatment on the structure, cavitation erosion and erosion-corrosion behavior of Fe-based amorphous coatings. *Tribol. Int.* **2015**, *90*, 393–403. [CrossRef]
21. Qiao, L.; Wu, Y.P.; Hong, S.; Zhang, J.F.; Shi, W.; Zheng, Y.G. Relationships between spray parameters, microstructures and ultrasonic cavitation erosion behavior of HVOF sprayed Fe-based amorphous/nanocrystalline coatings. *Ultrason. Sonochem.* **2017**, *39*, 39–46. [CrossRef] [PubMed]
22. Cheng, J.B.; Wang, B.L.; Liu, Q.; Liang, X.B. In-situ synthesis of novel Al-Fe-Si metallic glass coating by arc spraying. *J. Alloys Compd.* **2017**, *716*, 88–95. [CrossRef]
23. *ASTM G32-10-Standard Test Method for Cavitation Erosion Using Vibratory Apparatus*; ASTM International: West Conshohocken, PA, USA, 2010.
24. Jonas, O.; Steltz, W.; Dooley, B. *Steam Turbine Efficiency and Corrosion: Effects of Surface Finish, Deposits*; Report 1003997; Electrical Power Research Institute (EPRI): Palo Alto, CA, USA, 2001.
25. Lin, J.R.; Wang, Z.H.; Lin, P.H.; Cheng, J.B.; Zhang, J.J.; Zhang, X. Microstructure and corrosion resistance of Fe-based coatings prepared by twin wires arc spraying process. *J. Therm. Spray Technol.* **2014**, *23*, 333–339. [CrossRef]
26. Sharma, P.; Majumdar, J.D. Surface characterization and mechanical properties evaluation of Boride-dispersed Nickel-based coatings deposited on copper through thermal spray routes. *J. Therm. Spray. Technol.* **2012**, *21*, 800–809. [CrossRef]
27. Cheng, J.B.; Zhao, S.; Liu, D.; Feng, Y.; Liang, X.B. Microstructure and fracture toughness of the FePSiB-based amorphous/nanocrystalline coatings. *Mater. Sci. Eng. A* **2017**, *696*, 341–347. [CrossRef]
28. Heni, W.; Vonna, L.; Fioux, P.; Vidal, L.; Haidara, H. Ultrasonic cavitation test applied to thin metallic films for assessing their adhesion with mercaptosilanes and surface roughness. *J. Mater. Sci.* **2014**, *49*, 6750–6761. [CrossRef]
29. Jiang, N.N.; Liu, S.H.; Chen, D.R. Effect of roughness and wettability of silicon wafer in cavitation erosion. *Chin. Sci. Bull.* **2008**, *53*, 2879–2885. [CrossRef]
30. Friction, Lubrication, and Wear Technology. In *ASM Handbook (Volume 18)*; ASM International: Materials Park, OH, USA, 1992; pp. 408–435.
31. Santa, J.F.; Espitia, L.A.; Blanco, J.A.; Romo, S.A.; Toro, A. Slurry and cavitation erosion resistance of thermal spray coatings. *Wear* **2009**, *267*, 160–167. [CrossRef]
32. Scardina, P.; Edwards, M. Prediction and measurement of bubble formation in water treatment. *J. Environ. Eng.* **2001**, *11*, 968–973. [CrossRef]